

Intracapsular accommodation mechanism in terms of lens curvature gradient

Veronica Lockett-Ruiz¹  | Rafael Navarro¹  | Norberto López-Gil² 

¹INMA, Spanish National Research Council, University of Zaragoza, Zaragoza, Spain

²Instituto Universitario de Investigación en Envejecimiento, Universidad de Murcia, Murcia, Spain

Correspondence

Veronica Lockett-Ruiz, INMA-CSIC, Universidad de Zaragoza, Zaragoza, Spain.
Email: vlockett@unizar.es

Funding information

HORIZON EUROPE Marie Skłodowska-Curie Actions, Grant/Award Number: 956720; Ministerio de Ciencia e Innovación, Grant/Award Number: PID2019-107058RB-I00/AEI/10.13039/501100011033

Abstract

The intracapsular accommodation mechanism (IAM) may be understood as an increase in the lens equivalent refractive index as the eye accommodates. Our goal was to evaluate the existence of an IAM by analysing observed changes in the inner curvature gradient of the lens. To this end, we fitted a gradient index and curvature lens model to published experimental data on external and nucleus geometry changes during accommodation. For each case analysed, we computed the refractive power and equivalent index for each accommodative state using a ray transfer matrix. All data sets showed an increase in the effective refractive index, indicating a positive IAM, which was stronger for older lenses. These results suggest a strong dependence of the lens equivalent refractive index on the inner curvature gradient.

KEYWORDS

accommodation, crystalline lens, equivalent refractive index, gradient index, Gullstrand, intracapsular accommodation mechanism, lens curvature

INTRODUCTION

In his speech *Hur Jag Fann Den Intrakapsulära Ackommodationsmekanismen*¹ ('How I found the intracapsular accommodation mechanism') at the Nobel Banquet in Stockholm on 10 December 1911, ophthalmologist Allvar Gullstrand explained his novel discovery of an optical mechanism that increased the change in lens refractive power during accommodation.

Gullstrand's intracapsular accommodation mechanism (IAM) was based on a four-surface crystalline lens model with one refractive index for the cortex and a different, higher index for the nucleus. Let us consider an unaccommodated homogeneous lens with the same external geometry as the four-surface unaccommodated lens and an equivalent refractive index, n_{eq} , that yields the same refractive power. When the eye accommodates, the curvature change in Gullstrand's proposed four-surface lens produced more power than the equivalent two-surface homogeneous lens (Figure 1), assuming all refractive indices remain constant. Put differently, to match the increase

in lens power of the four-surface lens during accommodation, the equivalent refractive index of the two-surface homogeneous lens should increase.² In Gullstrand's¹ words, 'Thus in the eye the total index [equivalent index] of the lens increases during accommodation, a truly remarkable situation although as we have seen, the total index is not a physical refractive index but an imaginary concept.'

Since Gullstrand's six-surface eye model, with two surfaces for the cornea and four surfaces for the crystalline lens, subsequent two-surface accommodating crystalline lens models have included an equivalent refractive index that increased during accommodation.³⁻⁵ Later, more complex accommodating eye models with gradient index (GRIN) lenses^{6,7} have shown that the presence of GRIN media boosts the increase in refractive power during accommodation, suggesting the presence of a positive IAM in non-human primate lenses.⁸

Other studies have questioned the existence of an IAM. In particular, Hermans et al.⁹ found that Gullstrand's accommodated eye model could overestimate the lens power since it did not account for the accommodative

This is an open access article under the terms of the [Creative Commons Attribution-NonCommercial-NoDerivs](https://creativecommons.org/licenses/by-nc-nd/4.0/) License, which permits use and distribution in any medium, provided the original work is properly cited, the use is non-commercial and no modifications or adaptations are made.

© 2024 The Authors. *Ophthalmic and Physiological Optics* published by John Wiley & Sons Ltd on behalf of College of Optometrists.

error (lag) typically present in the accommodated eye. Other eye models, such as Garner and Smith's GRIN lens,¹⁰ do not present an IAM. More recently, in-vivo Scheimpflug imaging¹¹ has shown less change in the radii of curvature of the surfaces of the lens nucleus during accommodation than was proposed by Gullstrand. In fact, depending on the rate of change of these inner curvatures, one could even observe the opposite of an IAM, that is, an 'intracapsular mechanism of disaccommodation'.² Table 1 shows the IAM values found for different eye models. The increase in equivalent refractive index per dioptre of accommodation (IAM > 0) varied between 0.00078 and 0.00141^{1,3,4} depending on the model used, in contrast with more recent studies that reported a more negligible increase.^{9,10}

Determining the presence of an IAM is relevant, not only for historical or scientific reasons but also for its potential application to the design of accommodative intraocular lenses. As explained above,² whether an IAM occurs and, if so, its magnitude, depends on the lens model being considered (see Table 1). Hence, it is crucial to use a realistic model to analyse the effect of the internal structure on the accommodating lens power. Since the distribution of the GRIN and changes with accommodation could strongly affect the IAM, and considering that Gullstrand's IAM can only occur in a non-homogeneous lens, then GRIN models seem appropriate for studying and understanding this phenomenon. Most previous models assumed a concentric shell configuration (see a list of the most significant GRIN models in Navarro⁶). Only the most recent GRIN models^{14,15} allowed modification of the inner curvature gradient, which has been shown

Key points

- The contribution of the intracapsular mechanism to the increase in power during accommodation is significantly lower than that predicted by Gullstrand, particularly for younger lenses.
- The gradient radius of curvature of the inner surfaces of the lens contributes to the refractive power change during accommodation, having a multiplicative effect with the change in refractive index distribution.
- For lens models with a gradient refractive index and radius of curvature, the intracapsular accommodation mechanism is positive and increases between 18 and 45 years of age.

to enhance both lens power and amplitude of accommodation.⁷ The Accommodating volume-constant age-dependent optical (AVOCADO) model¹⁴ allowed changes to the curvature gradient, although indirectly. To our knowledge, only the GRINCU (double gradient: refractive index and radius of curvature) lens model¹⁵ provided an explicit and direct way to modify the inner curvature gradient, thus allowing a better fit of experimental data.

This study aimed to discover whether the human eye has an IAM as defined by Gullstrand. In other words, to solve the question: if the crystalline lens were assumed to be homogeneous, then should its equivalent index increase during

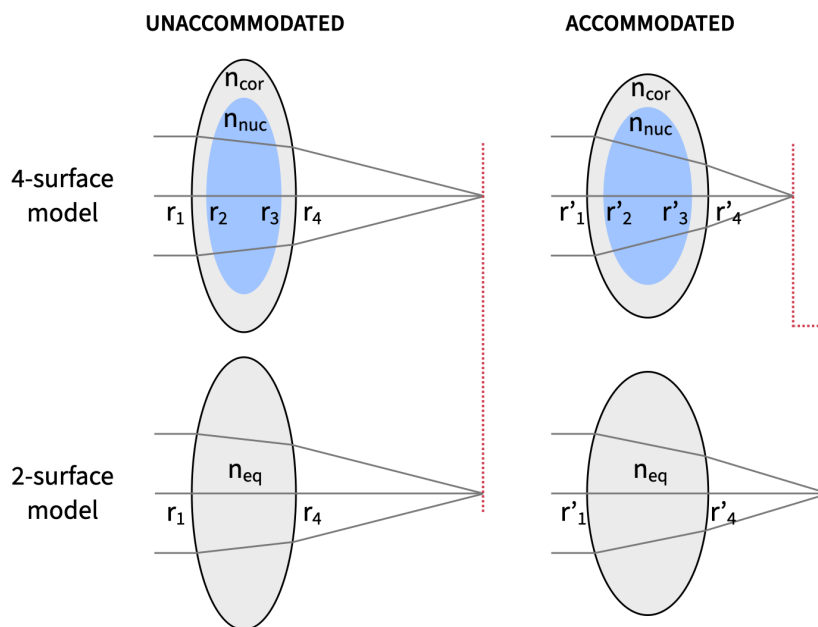


FIGURE 1 Intracapsular accommodation mechanism. Assuming that the two-surface unaccommodated lens (bottom-left) has an equivalent refractive index that confers the same power as the four-surface unaccommodated lens (top-left), then the accommodated four-surface lens (top-right) has a higher power than the two-surface lens (bottom-right), assuming their refractive indexes do not change during accommodation. Primed variables correspond to accommodated values. cor, cortex; eq, equivalent; *n*, refractive index; nuc, nucleus; *r*, radius of curvature.

TABLE 1 Comparison of the refractive power and equivalent refractive index changes across different accommodating eye studies and models.

Study	Lens model	Unaccommodated		Accommodated		Variation, $\Delta n_{eq}/\Delta P (10^{-3})$	IAM
		$P (D)$	n_{eq}	$P (D)$	n_{eq}		
Gullstrand ¹	4 surfaces	19.11	1.4085	33.06	1.4260	1.25	+
Le Grand ³	2 surfaces	21.78	1.420 0	30.70	1.4270	0.78	+
Navarro ⁴	2 surfaces	21.55	1.42	34.30	1.438	1.41	+
Hermans ⁹	4 surfaces	–	1.4345	–	1.4345	0	No
Garner ¹⁰	GRIN	21.75	1.4277	30.65	1.4277	0	No

Note: D, dioptres; GRIN, gradient index; IAM, intracapsular accommodation mechanism; n_{eq} , equivalent refractive index; P , power.

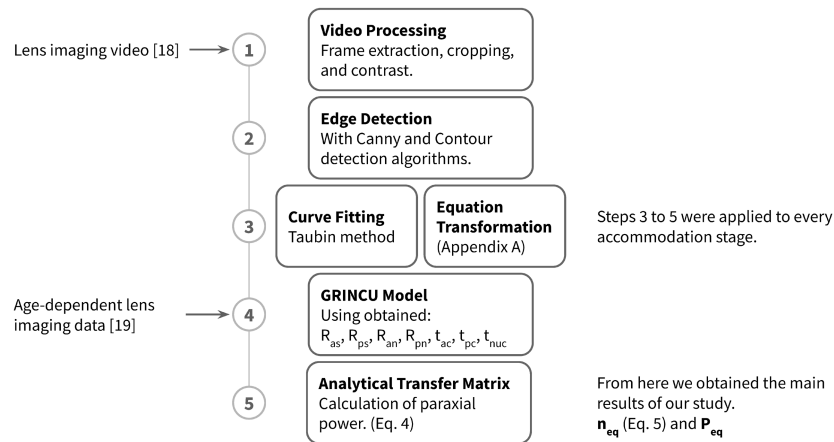


FIGURE 2 Flowchart showing the data analysis and result calculation process. Labels on the left illustrate at which point in the pipeline the data analysis started for each data set. ac, anterior cortex; an, anterior nucleus; as, anterior surface; eq, equivalent; GRINCU, double gradient: refractive index and radius of curvature; n , refractive index; nuc, nucleus; P , power; pc, posterior cortex; pn, posterior nucleus; ps, posterior surface; R , radius of curvature; t , thickness.

accommodation? To solve that question, we tested for the presence of an IAM in a GRINCU accommodative lens model, which we believe is especially well-suited to quantify an IAM accurately. Our departure hypothesis is that, together with the increase in curvature of the external lens surfaces, the inner shell curvature gradient change also plays an essential role in accommodation.⁷ Calculations in GRIN lens models may become complicated, but paraxial refraction accurately predicts clinical refraction¹² and the amplitude of accommodation.¹³ Therefore, paraxial optics is a suitable approximation to evaluate the presence of an IMA in accommodating GRIN lenses. Some proposed GRIN lens models^{14,15} have computed the paraxial power change during accommodation using ray tracing software or recursive algorithms that calculated the paraxial ray trajectories through each iso-indicial surface. Instead, we applied a powerful and straightforward method based on the (2-by-2) ray transfer matrix.^{16,17} We also analysed whether a four-surface model based on the datasets can accurately predict the IAM obtained by a more realistic GRIN model. Paraxial ray transfer matrix analysis was used in all cases to calculate the change in lens power and equivalent refractive index during accommodation, substantially simplifying the calculations.

To conduct this analysis, we used two independent sets of published experimental data on the change in lens geometry during accommodation.^{18–22}

METHODS

To evaluate the IAM in the GRINCU crystalline lens, we computed the power increase and the equivalent refractive index, representing, as far as we are aware, the first two sources in the literature with experimental geometry data for the lens nucleus surface. See Figure 2 for an overview of the steps taken to complete the analysis.

The first data set was obtained from an in-vivo accommodation recording of the external and internal lens geometry obtained with a Topcon SL-45 Scheimpflug camera (topconhealthcare.com) with a charge-coupled device (CCD) attachment replacing the film. It shows the lens of a 16-year-old individual disaccommodating from a maximum accommodation stimulus of 10.4D.¹⁸

The second data set was obtained from a study of 100 participants, with subject ages spread evenly between 18 and 70 years.¹⁹ Scheimpflug photographic data was collected at 2D intervals from zero to the maximum accommodation stimulus for all subjects. Lens radii of curvature and thicknesses were extracted for all ages and accommodation states, yielding a set of seven age- and accommodation-dependent equations describing the external and nucleus geometry of the lens.^{20–22} Therefore, this second data set indicated the average trend in a group

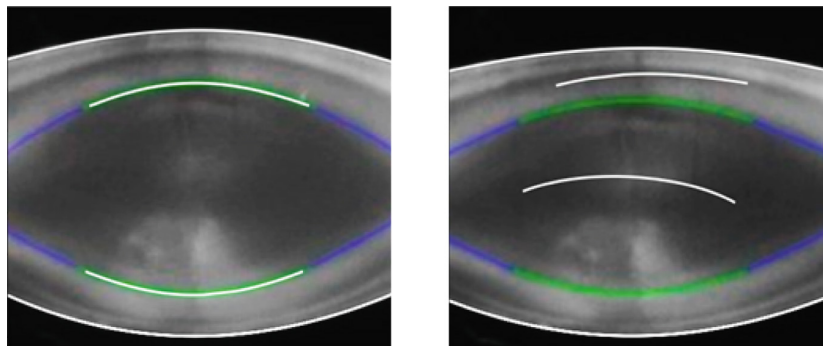


FIGURE 3 Example of fits that were included or excluded from the analysis. The detected contours appear as white curves overlaying the original images. The four fits on the left were included, whereas only the external surface fits on the right image were included.

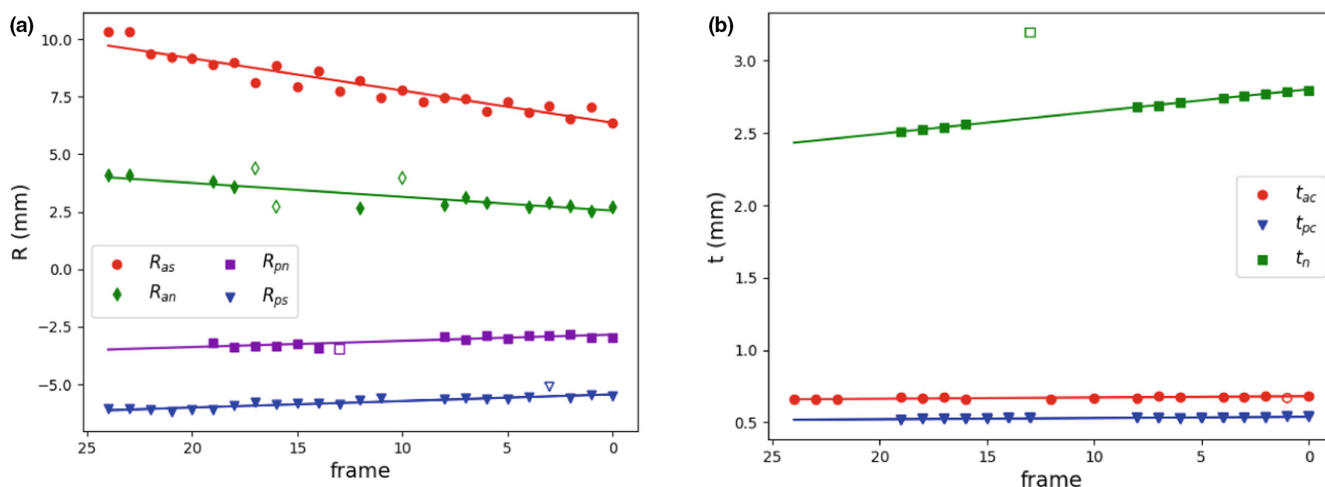


FIGURE 4 Linear regression fits obtained from fitting the Scheimpflug video contours. The solid markers represent the data, the empty markers show the points outside the confidence interval and the solid line is the best-fit line. (a) Radii of curvature (R) of the lens's four surfaces. R_{as} and R_{ps} are for the external anterior and posterior surfaces; R_{an} and R_{pn} are for the anterior and posterior nucleus surfaces. (b) Thickness (t) of the anterior cortex, t_{ac} , posterior cortex, t_{pc} and nucleus t_n . ac, anterior cortex; an, anterior nucleus; as, anterior surface; mm, millimetres; n, nucleus; pc, posterior cortex; pn, posterior nucleus; ps, posterior surface.

of 100 lenses, as opposed to the first data set, which was drawn from a single individual.

16-year-old lens: video processing and curve fitting

The first in-vivo experimental measurement data were downloaded as a Scheimpflug greyscale video from the online article (movie 2 in Hermans et al.¹⁸) and processed with Python²⁸ and OpenCV²⁹ to extract the coordinates of the accommodating surfaces. The authors had already corrected their published video for two types of distortion: Type I, due to the inclined position of the CCD camera and Type II, caused by refraction through the cornea and anterior lens surface. The surfaces of the nucleus had also been fitted to central conics with the Levenberg–Marquardt method.¹⁸ Therefore, no further corrections were applied to these data. The fitted nuclear boundaries appear as a green overlay in the published video. To extract

the Cartesian coordinates of the surfaces of the lens, we analysed the video in four steps:

1. The video frames were extracted, numbered, cropped to centre the crystalline lens and saved as a JPG file. The size of the video frames was 166 by 187 pixels.
2. The two external surfaces were mapped with Canny edge detection,²³ followed by a contour detection algorithm, which returns a set of curves joining all the continuous points along the boundary.
3. For the nucleus, the author's fit, shown as a green contour in the video, was used to map the lines. We applied a green mask, eroded the edge and used the contour detection function to find the boundary at each accommodative stage. All functions used in steps 1–3 were in the OpenCV Python package (Canny, findContours, drawContours, cvtColor and erode).
4. Finally, the unaccommodated thickness of the nucleus provided by Hermans et al.,¹⁸ that is, 2.48 mm, was used to calculate the pixel-to-mm ratio for the images. For all

of the processed images, the origin of the coordinate system was set at the (0, 0) pixel.

At this point in the analysis, each of the four lens surfaces at each accommodation stage in the video data was a contour defined by a set of (z -axial, ω -radial) coordinates. There were four contours for each accommodation step or video frame, adding up to 100. To obtain the surfaces' radii of curvature and conic constants, we applied Taubin's method for ellipse fitting²⁴ (A), followed by an equation transformation²⁵ to convert the quadric implicit equation to its canonical version (B). There were two main features of this fitting algorithm that make it especially suitable for conic fitting:

- It uses linear least squares, which makes it simple and guarantees both convergence and a unique solution.
- It uses a coordinate normalisation that strongly enhances its robustness against displacements in the 3D space. Furthermore, such normalisation has also shown (in an unpublished study from our laboratory) high accuracy in estimating the radius and conic constants even in reduced conic cords.

The video data yielded several high-error fits (>20% error), which were excluded. All fits were included for the anterior external surface; two fits were excluded for the posterior external surface, nine for the anterior nucleus surface and eight for the posterior. The errors of all included fits were <0.4% for all surfaces analysed. Figure 3 shows examples of included and excluded fits.

The resulting radii of curvature as well as cortex and nucleus thicknesses are plotted in Figure 4. The conic constants were not needed to compute paraxial lens power and were not included. Note that the frame order is reversed in all figures to show increasing accommodation. After computing a trend line for these more or less correlated clouds of data, we optimised the linear regression by removing the points outside a confidence interval of $\pm 1.8\sigma$ and recalculated the slope and intercept, significantly improving the R^2 value (see Table 2).

Age-dependent data

The external and nucleus geometry parameter equations of the lens for the age-dependent data were obtained directly

from published studies: rate of change of lens cortex and nucleus thickness with accommodation,²⁰ radii of curvature at zero-dioptres²¹ and with accommodation.²² All equations were in the form $y = y_0 + m_A \cdot \text{age} + (m_B + m_C \cdot \text{age}) \cdot D$, where age is in years and D is the accommodation demand in dioptres (see Table 3). Values were calculated for 18-, 29- and 45-year-old accommodating lenses with accommodation stimuli between 0 and 9D.

GRINCU model

The GRINCU model¹⁵ is a general, adaptive, age-dependent crystalline lens model that includes a gradient index (GRIN) and a gradient radius of curvature of the iso-indicial surfaces (GRCU); see Figure 5. The refractive index in the anterior and posterior regions of the lens varies as a function of the iso-indicial parameter, $z_0(z, \omega)$:

$$n(z_0) = \begin{cases} n_c + \delta n \cdot \left(1 - \frac{z_0}{t_a}\right)^p & \text{for } 0 \leq z_0 \leq t_a \\ n_c + \delta n \cdot \left(\frac{z_0 - t_a}{t_p}\right)^p & \text{for } t_a < z_0 \leq t \end{cases} \quad (1)$$

where n_c is the maximum refractive index at the centre of the lens, $\delta n = n_s - n_c$ is the refractive index difference between the lens surface and centre and t, t_a, t_p are the total, anterior and posterior thickness of the lens, respectively ($t_a + t_p = t$); p is an age-dependent parameter⁶: $p = 2.85 \times (1.1 \cdot 10^{-7}) \times \text{age}$.⁴ The internal curvature gradient parameter G and the external geometry of the lens determine the iso-indicial surface (IIS) radius of the curvature profile. The apical radius of curvature at any given IIS is computed in the anterior and posterior cortex regions by (see equation 13 in Navarro et al.¹⁷):

$$R_a(z_0) = R_{as} - g_a z_0 \quad (2a)$$

$$R_p(z_0) = R_{ps} - g_p(z_0 - t) \quad (2b)$$

where R_{as} and R_{ps} are the anterior and posterior surface apical radii of curvature, respectively, R_{an} and R_{pn} are the respective radii for the nucleus and g_a and g_p are the net gradients

TABLE 2 Scheimpflug video linear regression parameters (data set 1).

	R_{as} (mm)	R_{ps} (mm)	R_{an} (mm)	R_{pn} (mm)	Q_{as}	Q_{ps}	t_{ac} (mm)	t_{pc} (mm)	t (mm)
Intercept	6.37	-5.44	2.55	-2.84	-3.10	-0.37	0.68	0.54	4.02
Slope ($\times 10^{-2}$)	14.0	-2.88	6.04	-2.71	-9.24	-3.67	-0.0873	-0.0854	-1.70
R^2	0.917	0.884	0.846	0.743	0.134	0.558	0.710	0.674	0.999

Note: The intercepts are for the first frame, which corresponded to the maximum accommodation stimulus of 10.4D. The first four columns correspond to the radius of curvature (R) of the anterior and posterior surfaces of the lens and the anterior and posterior surfaces of the nucleus. Q_{as} and Q_{ps} are the conic constants of the lens anterior and posterior surfaces, and t_{ac} , t_{pc} and t are the anterior cortex, posterior cortex and lens thicknesses.

Abbreviations: ac, anterior cortex; an, anterior nucleus; as, anterior surface; mm, millimetres; pc, posterior cortex; pn, posterior nucleus; ps, posterior surface.

TABLE 3 Scheimpflug photographic age and accommodation fits (data set 2).^{20–22}

	R_{as}	R_{ps}	R_{an}	R_{pn}	t_{ac}	t_{pc}	t_n
Intercept (mm)	11.155	-8.267	3.782	-3.500	0.571	0.593	2.096
m_A (10^{-2} mm/year)	-2.004	2.025	-0.5996	0.5537	1.2	0.5	-0.3
m_B (mm/D)	-0.4736	0.2788	-0.0776	0.1092	0.002	-	0.041
m_C (10^{-3} mm/D · year)	4.705	-4.375	-0.584	-1.010	-	-	-
Maximum accommodation values for data set 2							
18 years old	6.893	-5.758	3.084	-2.517	0.5890	0.5930	2.465
29 years old	7.539	-6.312	2.757	-2.620	0.9370	0.7380	2.378
45 years old	7.896	-6.618	2.577	-2.677	1.129	0.8180	2.330

Note: The intercept corresponds to an 18-year-old lens for an accommodation stimulus of 0D, and the values are valid for between 18 and 45 years of age. For comparison with the 16-year-old individual data, the maximum accommodation values corresponding to data set 2 have been added in the three bottom rows. The first four columns correspond to the radius of curvature (R) of the anterior and posterior surfaces of the lens and the anterior and posterior surfaces of the nucleus. t_{ac} , t_{pc} and t_n are the anterior cortex, posterior cortex and nucleus thicknesses (t).

Abbreviations: ac, anterior cortex; an, anterior nucleus; as, anterior surface; n, nucleus; pc, posterior cortex; pn, posterior nucleus; ps, posterior surface.

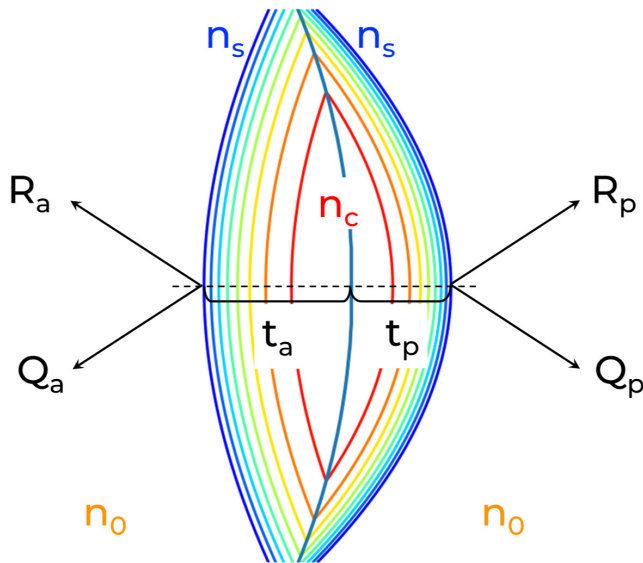


FIGURE 5 Illustrative example of a GRINCU lens. The external parameters R_a , R_p , Q_a and Q_p are the anterior and posterior surfaces' radii of curvature and the anterior and posterior surfaces' conic constants and define the internal geometry of the iso-indicial surfaces. The refractive indices at the lens surface and lens core, respectively, are denoted by n_s and n_c . We considered the same refractive index for the anterior chamber and vitreous humour, labelled n_o . Additionally, t_a and t_p represent the axial thickness of the anterior and posterior regions of the lens, respectively. a, anterior; p, posterior; s, surface.

of curvature ($g_a = G(Q_a + 1)$, $g_p = G(Q_p + 1)$). Using the lens geometry of the fitted lenses, we computed g_a and g_p .

$$g_a = \frac{R_{as} - R_{an}}{t_{ac}} \quad (3a)$$

$$g_p = \frac{R_{pn} - R_{ps}}{t_{pc}} \quad (3b)$$

where t_{ac} and t_{pc} are the anterior and posterior cortex thicknesses, respectively. The resulting net gradients of curvature

radius are high in both cases, especially for the anterior lens region, and decrease roughly linearly with accommodation (Figure 6). This steep decrease in radius of curvature towards the core may cause it to become zero or even reverse its sign inside the nucleus, which is theoretically and physiologically inconsistent. To avoid this potential problem, we used separate GRINCU configurations for the cortex and the nucleus. In the cortex, we applied the curvature gradients as calculated with Equation 3 and shown in Figure 6, and inside the nucleus, we consider zero gradient, that is, $R_a(z_0) = R_{an}$ and $R_p(z_0) = R_{pn}$ (inside the nucleus there is no gradient of curvature radius and the iso-indicial surfaces are parallel). Since the refractive index is approximately constant inside the nucleus, we can consider the nucleus as an almost homogeneous lens, and thus the assumption of constant curvature radii would not bias our paraxial power computation significantly.

Each accommodative stage was modelled in Python for the four datasets: the 16-year-old lens in the video data and the three different ages (18, 29 and 45) chosen from the age-dependent data set. We used refractive indices defined at 587.56 nm, $n_a = n_u = 1.3374$,⁶ $n_s = 1.3709$ and $n_c = 1.4181$ ²⁶ for the aqueous and vitreous humour, lens surface and lens core, respectively. The implementation of the model yielded an age- and external geometry-dependent refractive index distribution, index derivatives and iso-indicial surface profile for each accommodation stage.

Ray transfer matrix

The ABCD, or ray transfer matrix, provided a straightforward way to perform paraxial ray tracing and compute the cardinal points and power of a GRINCU lens.²⁷ This formulation considered the crystalline lens as an onion-type structure, with each IIS constituting a refracting optical surface. For any given layer of the onion-like structure, the ABCD matrix was the product of a translation and a refraction matrix. The complete lens ray transfer matrix was the product of the matrices of all layers inside

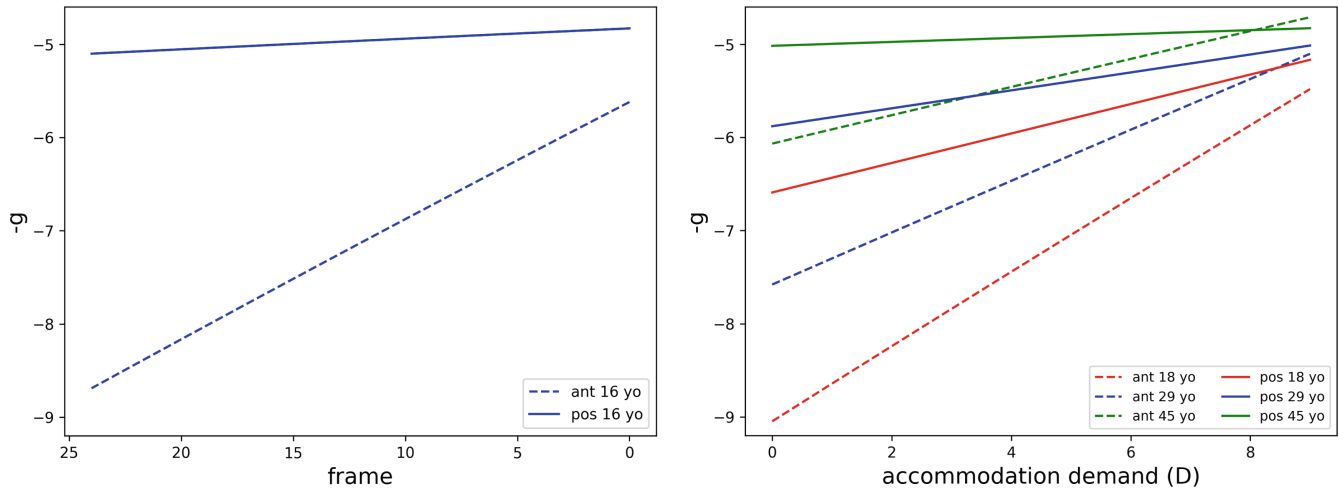


FIGURE 6 Anterior and posterior cortex net radius of curvature gradient (g) computed for the video (left) and age-dependent photographic data (right). The continuous line shows the posterior (pos) region gradient change, and the dashed line shows the anterior (ant) value.

the lens multiplied in the reverse order of the ray path. In the differential limit, when the layer thickness tends to zero, the elements of the resulting ABCD matrix were integrals.¹⁷ Under this approximation, the GRIN contribution to the power is additive; the lens power is the sum of the GRIN and lens surface contributions to the power.

$$P = P_S + P_G = P_S + \int_0^t \frac{n'(z)}{n(z)R(z)} dz \quad (4)$$

where P is the total lens power, and P_S and P_G are the lens surface and GRINCU contributions to the power. The surface power P_S was calculated with the standard homogeneous thick lens power equation using a refractive index equal to that of the surface $n_{\text{lens}} = n_s$ and the GRIN power P_G is given by an integral.¹⁷ To calculate the integral in Equation 4, we applied the trapezoidal rule of integration; Equation 1 was used to obtain the refractive index and its derivative $n'(s) = dn(s)/ds$, while Equations 2 and 3 were combined to calculate $R(s)$, replacing s_0 with s since the integral was calculated along the optical axis ($c=0$). For each of the four cases studied, we computed the paraxial power at each accommodation step.

The effective refractive index introduced by Gullstrand¹ was the index that an unaccommodated two-surface homogeneous lens would require in order to deliver the same refractive power as an unaccommodated GRIN (or four-surface) lens, assuming both had the same external geometry. This equivalent index is found by replacing the GRIN lens power in the lensmaker's equation.

$P = P_a + P_p - tP_aP_p/n_{\text{eq}}$ with $P_a = (n_{\text{eq}} - n_0)/R_{\text{as}}$ and $P_p = (n_0 - n_{\text{eq}})/R_{\text{ps}}$, where P_a and P_p are the anterior and posterior surface powers, then solving for n_{eq} :

$$n_{\text{eq}} = n_0 + \frac{n_0(R_{\text{as}} - R_{\text{ps}}) + PR_{\text{as}}R_{\text{ps}} - \sqrt{(PR_{\text{as}}R_{\text{ps}} - n_0(R_{\text{as}} - R_{\text{ps}}))^2 + 4n_0PR_{\text{as}}R_{\text{ps}}t}}{2(-R_{\text{as}} + R_{\text{ps}} + t)} \quad (5)$$

where n_{eq} is the equivalent refractive index, n_0 is the aqueous and vitreous humour refractive index, P is the unaccommodated total lens power, R_{as} and R_{ps} are the anterior and posterior surface radii of curvature and t is the lens thickness.

Finally, we calculated the equivalent power of a four-surface lens model with both a homogeneous cortex and nucleus. This lens model has two refractive indices: a refractive index n_c for the nucleus, equal to the central index of the GRINCU model and an equivalent refractive index n_{eqC} for the cortex, computed in such a way that the unaccommodated lens power was equal to that of a GRIN lens with the same external geometry. To compute the cortex equivalent refractive index in the four-surface model, we formulated a ray transfer matrix sequentially across the lens surfaces and media in reverse order of the ray path: $M = S_{\text{ps}}T_{\text{pc}}S_{\text{pn}}T_{\text{n}}S_{\text{an}}T_{\text{ac}}S_{\text{as}}$. Matrices $S_{\text{as}}, S_{\text{ps}}, S_{\text{an}}, S_{\text{pn}}$ represent refractions through the anterior and posterior external surfaces of the lens, and anterior and posterior surfaces of the nucleus, respectively; and, $T_{\text{ac}}, T_{\text{pc}}, T_{\text{n}}$ are the respective translation matrices across the anterior cortex, posterior cortex and nucleus. The paraxial refractive power of the four-surface lens was obtained by multiplying the matrix element M_{21} by the refractive index of the lens surrounding media, $P_{\text{eq},4} = n_0M_{21}$. To obtain the equivalent cortex index n_{eqC} , we optimised its value until $P_{\text{eq},4}$ matched the lens power P in the unaccommodated state.

RESULTS

For each accommodation stage in all of the cases studied, we computed the following in sequential order:

1. The anterior and posterior lens external and nucleus surfaces, the radius of curvature, the anterior and posterior cortex thicknesses and the total lens thickness. For the Scheimpflug age-dependent study (data set 2), parameters were calculated using the authors^{19–22} original fits (Table 3). For the Scheimpflug video¹⁸ (data set 1), we obtained these parameters (Figure 4 and Table 2) using the method described above.
2. The net radius of curvature gradient g (see Figure 6).
3. Implementation of the GRINCU model, using the geometrical parameters and curvature gradients obtained in points 1 and 2. The changes in the GRINCU

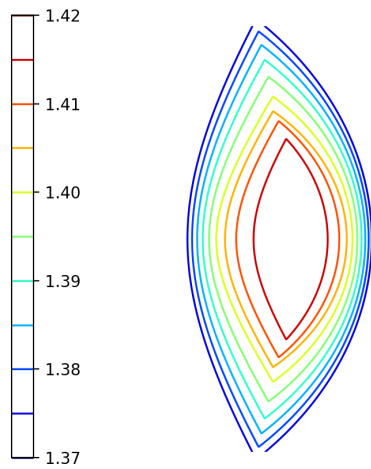


FIGURE 7 Accommodating iso-indicial surface (IIS) contours. Movie 1. Implementation of the double gradient: refractive index and radius of curvature (GRINCU) accommodation model based on Scheimpflug experimental video data.

4. The paraxial lens power of the GRINCU lens for each accommodative state, (Figure 8) and the corresponding equivalent refractive index (Figure 9) of a two-surface homogeneous lens of equal geometry.
5. The equivalent refractive index of a four-surface lens with homogeneous cortex and nucleus (Figure 10).

All accommodation cases showed similar trends in terms of lens geometry. The lens external and nucleus surface radii of curvature decreased with accommodation, with the anterior surface undergoing the most change (Figure 4a). The nucleus axial thickness increased the most compared with the anterior and posterior cortex thicknesses (Figure 4b). The net gradient g decreased in magnitude roughly linearly for all datasets and ages considered (Figure 6). In general, the anterior gradient varied the most, which can be explained by the significant radius of curvature decrease of the anterior lens surface and the almost negligible change in cortex thickness (see Equation 3). This asymmetry is the reason for the different change in g between the front and back surfaces of the lens (see Figure 6).

Figures 8 and 9 show the main results of this study. The refractive power increased monotonically (Figure 8), displaying a nearly quadratic trend with accommodation demand for all data sets. The total variation of lens power between the unaccommodated and fully accommodated states (solid lines) predicted by the GRINCU model varied from 9.64D for the 16-year-old individual in the experimental video to 5.86D for the 45-year-old participant in the age-dependent accommodation study data. The dashed lines in Figure 8 represent the power of a two-surface homogeneous lens model, computed with a constant equivalent

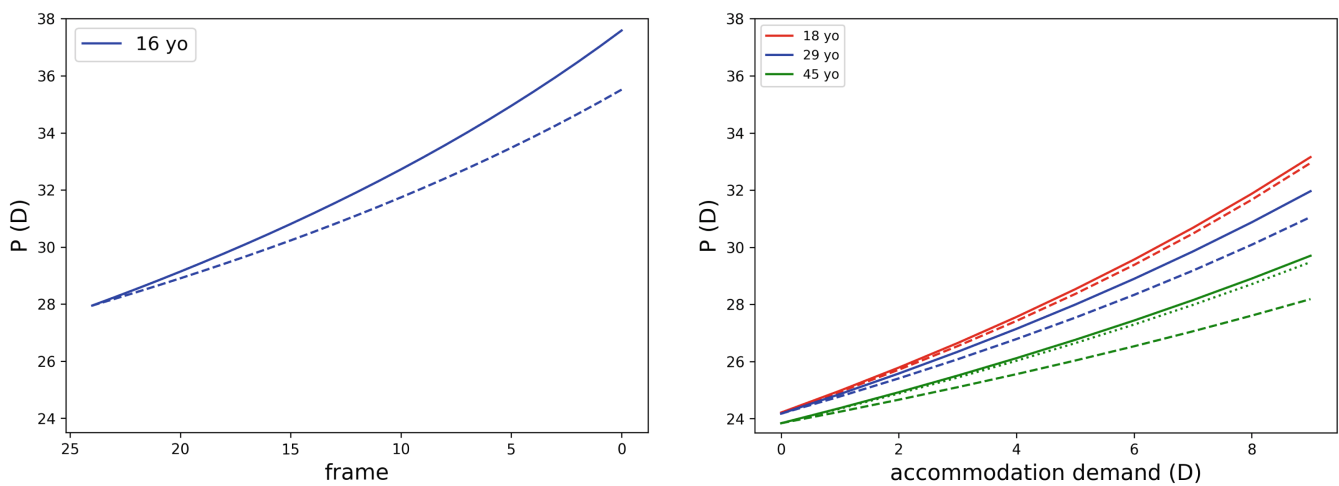


FIGURE 8 The two-surface homogeneous lens refractive power (dashed line) is lower than the refractive power computed for the double gradient: refractive index and radius of curvature (GRINCU) lens model (solid line), indicating a positive intracapsular accommodation mechanism (IAM) in all cases analysed. On the left, results are shown for the video and on the right, for the age-dependent study. P , power.

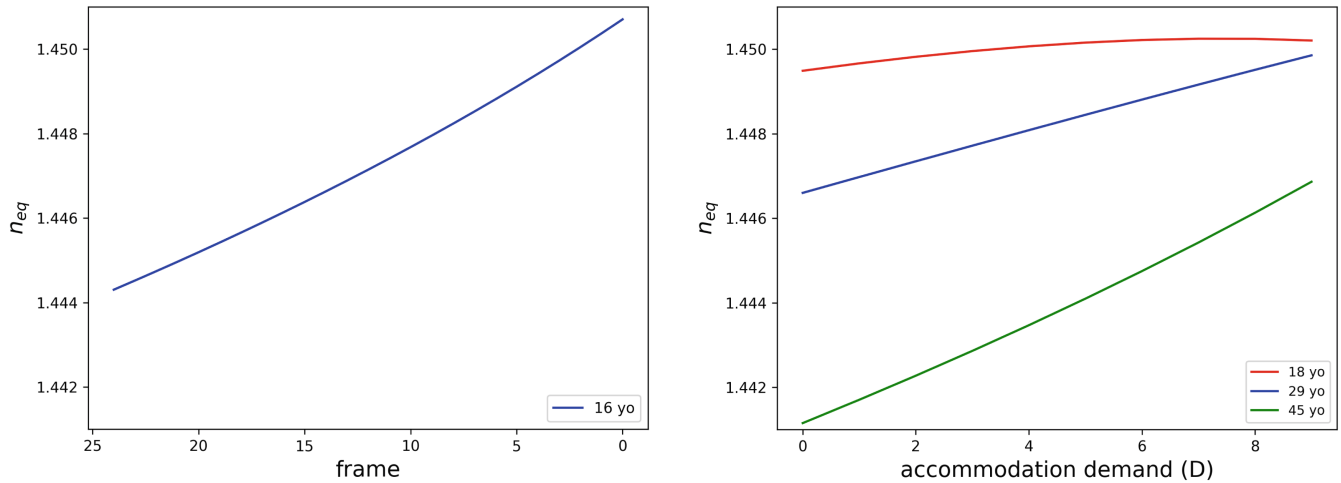


FIGURE 9 Equivalent refractive index (n_{eq}), computed at all accommodative stages for a two-surface homogeneous lens with the same external geometry as the double gradient: refractive index and radius of curvature (GRINCU) lens. On the left are the results for the video, and on the right are the results for the age-dependent study.

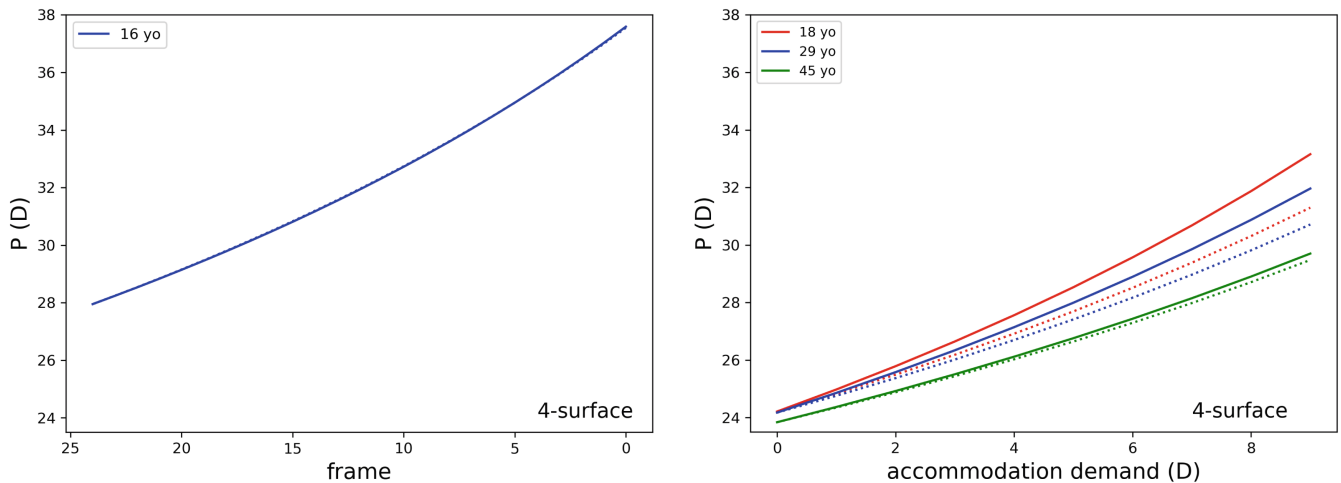


FIGURE 10 Lens refractive power computed with the double gradient: refractive index and radius of curvature (GRINCU) lens model (solid line) and for a four-surface lens with homogeneous cortex and homogeneous nucleus (dotted line). On the left, results are shown for the video and on the right, for the age-dependent study. P , power.

refractive index calculated for the unaccommodated state of the lens (Equation 5). According to Gullstrand's definition, for there to be an IAM, the actual power of the GRIN lens should increase more during accommodation than the power of its equivalent homogeneous lens. For all ages considered here, the homogeneous lens refractive power lay below the GRINCU lens power, thus establishing a positive IAM. Figure 8 (right panel) suggests that the IAM increases with age, which is confirmed by the equivalent index (Figure 9). The power of the four-surface model closely matched the GRINCU power in the experimental video data analysis (Figure 10, left), which could suggest that the four-surface and GRINCU models were equivalent. However, the results for the experimental age-dependent fits (Figure 10, right) were quite different since the

four-surface model yielded a positive IAM that decreased with age.

DISCUSSION

This analysis yielded a positive IAM in all cases, although with a different trend for the 18-year-old lens. The results of the age-dependent study (data set 2) suggest that the IAM did not decline with age but, on the contrary, appeared to increase from 18- to 45-year-old lenses. These results suggest that the contribution of the IAM to the total accommodation response is less than one-third in all cases studied (the highest contribution being 26% for the 45-year-old lens), which was lower than Gullstrand's

calculation. This moderate contribution might seem to contradict other results, at least for non-human primates, which indicated that the GRIN structure in the lens accounts for two-thirds of the total accommodation.⁸ However, there is no contradiction since the previous study⁸ defined the GRIN contribution to the lens power, P_G , as the difference between the total power (P) and the power of the anterior and posterior surfaces, P_S : $P_G = P - P_S$. To find the effect of the GRIN on accommodation, these authors calculated the power increase due to the GRIN structure only. Since P is linear with P_S and P_G (Equation 4), it is straightforward to obtain the increase in the GRIN contribution in terms of surface and total power increases:

$$\Delta P_G = \Delta P - \Delta P_S \tag{6}$$

where ΔP is the change in the total power of the lens and ΔP_S and ΔP_G are the increases in power contributions due to the surface and GRIN, respectively. Our model predicts unaccommodated ratios of P_G/P between 67% and 70% (see Table 4), which is consistent with the relative contributions reported by Hermans et al.⁹ While it is true that the GRIN structure contributed the most to accommodation, that itself does not guarantee an increase in the equivalent refractive index or a subsequent positive IAM. The present results suggest that a positive IAM requires that $\Delta P_G / \Delta P > P_G / P$, which would imply an increase in the equivalent refractive index (see Table 4). Indeed, the same authors found a strong

influence of the GRIN on the accommodation response⁸ with no change in the equivalent index of the lens during accommodation (IAM=0).

Table 5 compares the lens refractive power and equivalent refraction index change between the unaccommodated and fully accommodated states obtained in the present study. It is worth noting the different nature of the data on the first row (16-year-old lens), which corresponds to a single individual, and the last three rows, which represent average trends in a cohort of 100 eyes. Comparing Tables 1 and 5, the most significant equivalent refractive index increments correspond to simplified lens models with two or four surfaces, in contrast with more realistic GRIN or GRINCU models. The Le Grand eye model³ is an exception, as well as the findings of the Hermans et al. study,⁹ which accounted for the lag of accommodation and showed less change in lens power than the two or four-surface models. The difference between the variation in target vergence and the actual change in the accommodation response, that is, the accommodative error, could be essential in studying the effect of the IAM.⁹ Table 5 shows that all models demonstrated a positive IAM. Interestingly, the value for the 16-year-old individual¹⁸ (data set 1) was larger than for the 18-year-old from data set 2, even though the ages were similar. We believe that this discrepancy could be explained by the fact that one individual (data set 1) can differ quite significantly from the average trend (data set 2). Nevertheless, in all cases, we see that the GRINCU model showed a positive IMA for all ages, but the change in accommodation due to the GRIN structure of the lens was not as high as that proposed by Gullstrand.

Figure 11 illustrates the strong impact of the radius of curvature gradient g on the IAM. When $g=0$, the IAM was negligible since the power of the homogeneous two-surface lens model nearly matched the power of the GRINCU lens. At the same time, when $g=0$, almost 100% of the power increase was due to the change in surface curvature, and the GRIN contribution was negligible. In addition, note that both the lens power and the power increase with accommodation were low when compared with the findings shown in Figure 8. Therefore, to explain both lens power and the total increment of lens power with accommodation, one must consider not only the change in surface curvatures but also the inner shells' radius of curvature gradient

TABLE 4 Power ratios for all cases analysed.

	16 yo (Video)	18 yo (Age-dependent study)	29 yo	45 yo
P_G/P unaccommodated	68.30%	69.81%	69.00%	67.36%
$\Delta P_G/\Delta P$	74.44%	69.89%	72.01%	75.27%
IAM sign	+	+	+	+

Note: P_G is the GRIN contribution to the unaccommodated lens power, P is the unaccommodated lens power, ΔP_G is the increase in GRIN power with accommodation and ΔP is the increase in total lens power. The more the GRIN contributed to accommodation when compared with the unaccommodated state, then the greater the IAM observed. In other words, the observed IAM was stronger the greater $\Delta P_G/\Delta P$ was relative to P_G/P .

Abbreviations: IAM, intracapsular accommodation mechanism; yo, years old.

TABLE 5 Comparison of the refractive power and equivalent refractive index changes in the studied GRIN models.

Study	Unaccommodated		Accommodated		Variation, $\Delta n_{eq}/\Delta P (10^{-3})$	IAM
	$P (D)$	n_{eq}	$P (D)$	n_{eq}		
GRINCU, 16 yo ^a	27.95	1.4443	37.59	1.4507	0.664	+
GRINCU, 18 yo ^b	24.21	1.4495	33.16	1.4502	0.078	+
GRINCU, 29 yo ^b	24.17	1.4466	31.96	1.4499	0.424	+
GRINCU, 45 yo ^b	23.84	1.4412	29.70	1.4469	0.972	+

Abbreviations: D, dioptres; GRINCU, double gradient: refractive index and radius of curvature; IAM, intracapsular accommodation mechanism; n_{eq} , equivalent refractive index; P , power.

^aData set 1 (one eye).

^bData set 2 (100-eyes average).

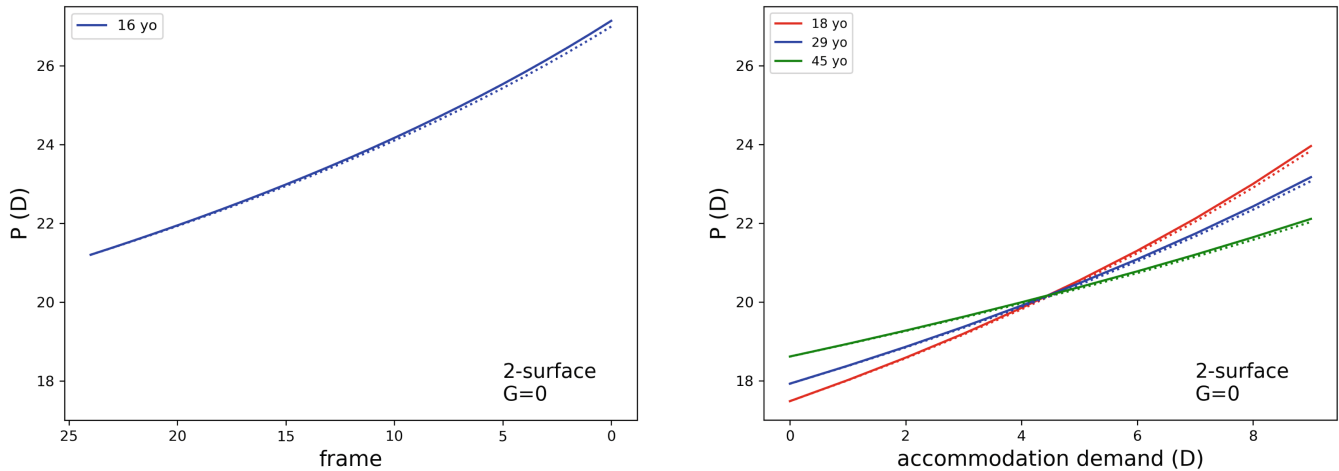


FIGURE 11 Lens refractive power calculated without a radius of curvature gradient ($G=0$). On the left, results are shown for the 16-year-old subject and on the right, for the age-dependent study. The solid line depicts the paraxial refractive power, and the dotted lines correspond to the equivalent power of a two-surface homogeneous lens model. P , power.

g . These findings confirm our departure hypothesis linking the IAM to the change in radius of curvature gradient with accommodation. What is new in the GRINCU model is that it provides an explicit quantitative explanation of the contribution of the inner lens shells' radius of curvature to the refractive power. Equation 4 indicates that the GRIN contribution to the power is additive and comprises the sum of each shell's contribution to the power. This contribution was proportional to the gradient index derivative n' and the shell curvature ($1/R$), meaning that both the GRIN and inner curvature are equally important and have a common multiplicative effect.⁷ The power contributed by each (differential) layer was similar to the power of a standard lens surface. The increase in lens power with accommodation results from the changes in index distribution and lens geometry. The only change in the index distribution with accommodation was the stretching of the index profile as the lens thickened (Equation 1). This predicts a slight decrease in n' and hence a small reduction in lens power (integrand in Equation 4). However, R and g vary greatly with accommodation, and so the increase in lens power must be mainly due to the change of these two parameters (anterior and posterior).

To summarise, we found a positive intracapsular accommodation mechanism as reported by most previous studies (see Tables 1 and 5). This confirms Gullstrand's finding, although the magnitude of the IAM observed in the present study was significantly lower, especially for the younger lenses. Interestingly, the results of the present study show a clear trend for the IAM to increase substantially with age. This increase with age could be a way to partially compensate for the decrease in accommodation response with age. However, further studies would be necessary to confirm this finding.

AUTHOR CONTRIBUTIONS

Veronica Lockett-Ruiz: Conceptualization (equal); formal analysis (equal); investigation (equal); methodology (equal); writing – original draft (equal); writing – review and editing (equal). **Rafael Navarro:** Conceptualization (equal); formal

analysis (equal); investigation (equal); methodology (equal); writing – original draft (equal); writing – review and editing (equal). **Norberto Lopez-Gil:** Conceptualization (equal); formal analysis (equal); investigation (equal); methodology (equal); writing – original draft (equal); writing – review and editing (equal).

FUNDING INFORMATION

Funded by the European Union's Horizon 2020 research and innovation programme under the Marie Skłodowska-Curie grant agreement No 956720 and by the Agencia Estatal de Investigación, Ministerio de Ciencia e Innovación y Universidades of Spain (MICIN), grant number PID2019-107058RB-I00/AEI/10.13039/501100011033CONFLICTS OF INTEREST.

CONFLICT OF INTEREST STATEMENT

The authors declare no conflicts of interest.

ORCID

Veronica Lockett-Ruiz  <https://orcid.org/0000-0002-9413-838X>

Rafael Navarro  <https://orcid.org/0000-0002-1328-1716>

Norberto López-Gil  <https://orcid.org/0000-0002-6696-4596>

REFERENCES

- Gullstrand A. How I found the mechanism of intracapsular accommodation. *Nobel Lecture*. 1911;383–415.
- López-Gil N. Gullstrand intracapsular accommodation mechanism revised. *Photonics* 2022;9:152. <https://doi.org/10.3390/photonics9030152>.
- LeGrand Y, ElHage SG. *Physiological optics*. Vol 13. Berlin: Springer; 2013.
- Navarro R, Santamaria J, Bescós J. Accommodation-dependent model of the human eye with aspherics. *J Opt Soc Am A*. 1985;2:1273–80.
- Zapata-Díaz JF, Radhakrishnan H, Charman WN, López-Gil N. Accommodation and age-dependent eye model based on in vivo measurements. *J Optom*. 2019;12:3–13.

6. Navarro R. Adaptive model of the aging emmetropic eye and its changes with accommodation. *J Vis.* 2014;14:21. <https://doi.org/10.1167/14.13.21>
7. Navarro R, López-Gil N. Impact of internal curvature gradient on the power and accommodation of the crystalline lens. *Optica.* 2017;4:334–40.
8. Maceo BM, Manns F, Borja D, Nankivil D, Uhlhorn S, Arrieta E, et al. Contribution of the crystalline lens gradient refractive index to the accommodation amplitude in non-human primates: in vitro studies. *J Vis.* 2011;11:23. <https://doi.org/10.1167/11.13.23>
9. Hermans EA, Dubbelman M, Van der Heijde R, Heethaar RM. Equivalent refractive index of the human lens upon accommodative response. *Optom Vis Sci.* 2008;85:1179–84.
10. Garner LF, Smith G. Changes in equivalent and gradient refractive index of the crystalline lens with accommodation. *Optom Vis Sci.* 1997;74:114–9.
11. Dubbelman M, Van der Heijde G, Weeber HA, Vrensen G. Changes in the internal structure of the human crystalline lens with age and accommodation. *Vision Res.* 2003;43:2363–75.
12. Thibos LN, Hong X, Bradley A, Applegate RA. Accuracy and precision of objective refraction from wavefront aberrations. *J Vis.* 2004;4:329–51.
13. López-Gil N, Fernández-Sánchez V, Thibos LN, Montés-Micó R. Objective amplitude of accommodation computed from optical quality metrics applied to wavefront outcomes. *J Optom.* 2009;2:223–34.
14. Sheil CJ, Goncharov AV. Accommodating volume-constant age-dependent optical (AVOCADO) model of the crystalline GRIN lens. *Biomed Opt Express.* 2016;7:1985–99.
15. Navarro R, Baquedano S, Sánchez-Cano AI. GRINCU lens with conicoid iso-indicial surfaces: application for modeling the crystalline lens. *Opt Express.* 2021;29:30998–31009.
16. Díaz JA. ABCD matrix of the human lens gradient-index profile: applicability of the calculation methods. *Appl Optics.* 2008;47:195–205.
17. Navarro R, Lockett-Ruiz V, López JL. Analytical ray transfer matrix for the crystalline lens. *Biomed Opt Express.* 2022;13:5836–48.
18. Hermans E, Dubbelman M, van der Heijde R, Heethaar R. The shape of the human lens nucleus with accommodation. *J Vis.* 2007;7:16. <https://doi.org/10.1167/7.10.16>
19. Koretz JF, Kaufman PL, Neider MW, Goeckner PA. Accommodation and presbyopia in the human eye—aging of the anterior segment. *Vision Res.* 1989;29:1685–92.
20. Koretz JF, Cook CA, Kaufman PL. Accommodation and presbyopia in the human eye. Changes in the anterior segment and crystalline lens with focus. *Invest Ophthalmol Vis Sci.* 1997;38:569–78.
21. Koretz JF, Cook CA, Kaufman PL. Aging of the human lens: changes in lens shape at zero-diopter accommodation. *J Opt Soc Am A.* 2001;18:265–72.
22. Koretz JF, Cook CA, Kaufman PL. Aging of the human lens: changes in lens shape upon accommodation and with accommodative loss. *J Opt Soc Am A.* 2002;19:144–51.
23. Canny J. A computational approach to edge detection. *IEEE Trans Pattern Anal Mach Intell.* 1986;6:679–98.
24. Taubin G. Estimation of planar curves, surfaces, and nonplanar space curves defined by implicit equations with applications to edge and range image segmentation. *IEEE Trans Pattern Anal Mach Intell.* 1991;13:1115–38.
25. Korn GA, Korn TM. Mathematical handbook for scientists and engineers: definitions, theorems, and formulas for reference and review. New Chelmsford, MA: Courier Corporation; 2000.
26. Jones CE, Atchison DA, Meder R, Pope JM. Refractive index distribution and optical properties of the isolated human lens measured using magnetic resonance imaging (MRI). *Vision Res.* 2005;45:2352–66.
27. Gerrard A, Burch JM. Introduction to matrix methods in optics. New Chelmsford: Courier Corporation; 1994.
28. Van Rossum G, Drake FL. Python 3 Reference Manual. Scotts Valley, CA: CreateSpace; 2009.
29. Bradski G, Kaehler A. Learning OpenCV: Computer vision with the OpenCV library. Sebastopol, CA: O'Reilly Media, Inc.; 2008.

SUPPORTING INFORMATION

Additional supporting information can be found online in the Supporting Information section at the end of this article.

How to cite this article: Lockett-Ruiz V, Navarro R, López-Gil N. Intracapsular accommodation mechanism in terms of lens curvature gradient. *Ophthalmic Physiol Opt.* 2024;44:334–346. <https://doi.org/10.1111/opo.13271>

APPENDIX A

TAUBIN CURVE FITTING

Non-linear conic surface fitting algorithms may yield significantly biased conic constant estimates, especially when the available arc subtends a small fraction of the whole conic surface. To guarantee convergence, robustness and accuracy, we implemented Taubin's linear least squares ellipse fit method,²⁴ based on minimising the mean square distance between the data points and the conic, to fit the lens nucleus and external surfaces. In addition to the important advantages of linear least squares methods as compared with non-linear algorithms, it uses previous data normalisation, which is extremely powerful in providing stable and reliable estimates of all parameters, including the conic constant.

We assumed that the four surfaces of the lens were rotationally symmetric quadrics and that we could fit our two-dimensional contours to conic sections. Any bivariate quadratic curve can be written as a polynomial in powers of z and ω :

$$F_0 + F_1 z^2 + F_2 z\omega + F_3 \omega^2 + F_4 z + F_5 \omega = 0 \quad (A1)$$

Our goal was to find the F_n coefficients from which to compute the conic parameters, mainly the type of conic, the semiaxes and the principal axis orientation. Taubin's method for ellipse fitting requires that the data be normalised for the best fit. So first, we normalised the datasets using the mean values $\bar{z}, \bar{\omega}$ and standard deviations $\bar{\sigma}_z, \bar{\sigma}_\omega$. The normalised variables Z and Ω , with $Z = (z - \bar{z})\sqrt{2}/\bar{\sigma}_z$ and $\Omega = (\omega - \bar{\omega})\sqrt{2}/\bar{\sigma}_\omega$ make up a new bivariate polynomial with coefficients $a_n = a_n(F_n, \bar{z}, \bar{\omega}, \bar{\sigma}_z, \bar{\sigma}_\omega)$

$$a_0 + a_1 Z^2 + a_2 Z\Omega + a_3 \Omega^2 + a_4 Z + a_5 \Omega = 0 \quad (A2)$$

The use of a general formulation, which includes any possible position or orientation of the conic, together with the coordinate normalisation, makes the conic shape

parameters (R and Q) to be invariant, fully independent from the chosen origin of coordinates.

The least-square fitting of the matrix with columns $[Z^2, Z\Omega, \Omega^2, Z, \Omega]$ yielded the values of coefficients a_0 to a_5 . We then rearranged Equation A2 to de-normalise the variables and compute F_0 through F_5 . With the F_n coefficients of the now adjusted surfaces, we finally rebuild the ellipses and calculate the fit error. The cortex and lens thicknesses can be computed by calculating the distance between the intersections of the curves with the principal axis. The final step for obtaining the required curve parameters was to convert the conic implicit equation to its canonical form (B).

IMPLICIT TO CANONICAL CONIC EQUATION TRANSFORMATION

The axial radius of curvature and conic constant of a central conic (ellipse or hyperbola) were calculated from the semi-axes: $R = b^2/a$ and $Q = sb^2/a^2 - 1$, where $s < -1$ for hyperbolas and $s > -1$ for ellipses. In the case of parabolas, $s = 0$, $Q = -1$ and the radius of curvature is $R = 2p$, where p is the distance between the vertex and the focus. To convert the implicit equation to its canonical form, we applied the matrix representation of conic sections.²⁵ The determinant of the equation matrix, A , the determinant of element A_{33} , $D = |A_{33}|$ and its trace, $I = \text{tr}(A_{33})$ are invariant to rotation and translation and define quadri properties that are independent of its position.

$$A = \begin{vmatrix} F_1 & F_2/2 & F_4/2 \\ F_2/2 & F_3 & F_5/2 \\ F_4/2 & F_5/2 & F_0 \end{vmatrix} \quad (\text{B3})$$

$$D = |A_{33}| = F_1 F_3 - \frac{F_2^2}{4} = \begin{cases} D > 0 & \text{for ellipses} \\ D = 0 & \text{for parabolas} \\ D < 0 & \text{for hyperbolas} \end{cases} \quad (\text{B4})$$

$$I = F_1 + F_3 \quad (\text{B5})$$

Invariants A, D, I and the roots of the characteristic equation $\beta^2 - I\beta + D = 0$ allow us to calculate the squared semi-axes of the conic, a^2 and b^2 , or the semilatus rectum for parabolas.

$$\text{Ellipses} \begin{cases} a^2 = \frac{-A}{\lambda_2 D} \\ b^2 = \frac{-A}{\lambda_1 D} \end{cases} \quad (\text{B6})$$

$$\text{Hyperbolas} \begin{cases} a^2 = \frac{-A}{\lambda_1 D} \\ b^2 = \frac{A}{\lambda_2 D} \end{cases} \quad (\text{B7})$$

$$\text{Parabolas: } p = \frac{1}{2} \sqrt{\frac{-A}{I^3}} \quad (\text{B8})$$

If there are no cross terms in the implicit equation, then $F_2 = 0$, and there are two possible orientations for the principal axis of the conic. If $F_1 < F_3$, the conic central axis is along s , but if $F_1 > F_3$, it is at $\pi/2$ rad from the positive z -axis. Therefore, to calculate R and Q correctly, a and b need to be swapped in the equations $R = a^2/b$ and $Q = a^2/b^2 - 1$.